



Extracellular CIRP Induces an Inflammatory Phenotype in Pulmonary Fibroblasts *via* TLR4

Siavash Bolourani^{1,2,3}, Ezgi Sari¹, Max Brenner^{1,2,3,4*} and Ping Wang^{1,2,3,4*}

¹ Center for Immunology and Inflammation, Feinstein Institutes for Medical Research, Manhasset, NY, United States, ² Elmezzi Graduate School of Molecular Medicine, Manhasset, NY, United States, ³ Department of Surgery, Donald and Barbara Zucker School of Medicine at Hofstra/Northwell, Manhasset, NY, United States, ⁴ Department of Molecular Medicine, Donald and Barbara Zucker School of Medicine at Hofstra/Northwell, Manhasset, NY, United States

OPEN ACCESS

Edited by:

Guo-Chang Fan,
University of Cincinnati,
United States

Reviewed by:

Qun Zang,
Loyola University Chicago,
United States
Guirong Wang,
Upstate Medical University,
United States
Samithamby Jey Jeyaseelan,
Louisiana State University,
United States

*Correspondence:

Ping Wang
pwang@northwell.edu
Max Brenner
mbrenner@northwell.edu

[†]These authors have contributed
equally to this work and
share senior authorship

Specialty section:

This article was submitted to
Inflammation,
a section of the journal
Frontiers in Immunology

Received: 07 June 2021

Accepted: 09 July 2021

Published: 23 July 2021

Citation:

Bolourani S, Sari E, Brenner M and
Wang P (2021) Extracellular CIRP
Induces an Inflammatory Phenotype in
Pulmonary Fibroblasts *via* TLR4.
Front. Immunol. 12:721970.
doi: 10.3389/fimmu.2021.721970

Extracellular cold-inducible RNA-binding protein (eCIRP), a new damage-associated molecular pattern (DAMP), has been recently shown to play a critical role in promoting the development of bleomycin-induced pulmonary fibrosis. Although fibroblast activation is a critical component of the fibrotic process, the direct effects of eCIRP on fibroblasts have never been examined. We studied eCIRP's role in the induction of inflammatory phenotype in pulmonary fibroblasts and its connection to bleomycin-induced pulmonary fibrosis in mice. We found that eCIRP causes the induction of proinflammatory cytokines and differentially expression-related pathways in a TLR4-dependent manner in pulmonary fibroblasts. Our analysis further showed that the accessory pathways MD2 and Myd88 are involved in the induction of inflammatory phenotype. In order to study the connection of the enrichment of these pathways in priming the microenvironment for pulmonary fibrosis, we investigated the gene expression profile of lung tissues from mice subjected to bleomycin-induced pulmonary fibrosis collected at various time points. We found that at day 14, which corresponds to the inflammatory-to-fibrotic transition phase after bleomycin injection, TLR4, MD2, and Myd88 were induced, and the transcriptome was differentially enriched for genes in those pathways. Furthermore, we also found that inflammatory cytokines gene expressions were induced, and the cellular responses to these inflammatory cytokines were differentially enriched on day 14. Overall, our results show that eCIRP induces inflammatory phenotype in pulmonary fibroblasts in a TLR4 dependent manner. This study sheds light on the mechanism by which eCIRP induced inflammatory fibroblasts, contributing to pulmonary fibrosis.

Keywords: fibroblast, eCIRP, inflammation, fibrosis, bleomycin

INTRODUCTION

Extracellular cold-inducible RNA-binding protein (eCIRP), a novel damage-associated molecular pattern (DAMP) discovered by our lab, plays a key role in sepsis, hemorrhagic shock, ischemia-reperfusion injuries (1–5). eCIRP induces these effects *via* its binding to and activation of the toll-like receptor 4 (TLR4) and myeloid differentiation factor 2 (MD-2) receptor complex (6). The role of

eCIRP in the activation of pulmonary cell populations such as macrophages (1), alveolar epithelial cells (7, 8), and endothelial cells (9) have been studied. However, the effect of eCIRP on pulmonary fibroblasts has yet to be studied.

Recently, we have discovered that eCIRP plays a role in the development of pulmonary fibrosis (publication forthcoming). Furthermore, a growing body of evidence suggests that blocking other DAMPs that also stimulate TLR4 can ameliorate pulmonary fibrosis (10–12). These factors have been shown to induce an inflammatory phenotype in fibroblasts through a TLR4 dependent process (13, 14) and that halting TLR4 dependent pathway alleviates the process of inflammatory fibroblast transformation (15–17). Fibroblasts are the key cells in the development of fibrosis in the lung. These mesenchymal cells are not terminally differentiated, and the principal regulator and potent inducer of fibroblast-to myofibroblast differentiation are transforming growth factor (TGF)- β (18–20). However, for persistent activation of fibroblasts to occur, TGF- β signaling needs to be enhanced by induction of a primed cellular microenvironment (21–24). A variety of signals and receptors have been shown to aid fibroblasts proliferation and cellular differentiation (25–29). However, the role of eCIRP on pulmonary fibroblasts has yet to be elucidated.

Inflammatory fibroblasts have been studied in various pathological processes such as neoplastic differentiation, autoimmune diseases, and fibrosis (30–32). Multiple factors have been implicated in the induction of inflammatory fibroblasts, such as mechanical stress, immunoglobulins, cytokines, and DAMPs (33–40). A growing body of evidence suggests that many factors that induce inflammatory fibroblast transformation operate in a TLR4 dependent manner (13–17). In this work, we examined the transcriptional response of pulmonary fibroblasts stimulated with eCIRP *in vitro*, focusing on proinflammatory, TLR4-induced pathways. We then evaluated how these pathways change over the course of bleomycin-induced pulmonary fibrosis.

MATERIALS AND METHODS

Pulmonary Fibroblast Isolation and Culture

Wild type (WT) C57BL/6 mice and TLR4^{-/-} mice (Jackson Labs, on a C57BL/6 genetic background) were used in this study. All experiments involving live animals were carried out in accordance with the National Institutes of Health guidelines for the use of experimental animals (41) and were reviewed and approved by the Institutional Animal Care and Use Committee (IACUC) at the Feinstein Institutes for Medical Research. The lungs of 4–8-week-old WT and TLR4^{-/-} mice were explanted, and each group of pulmonary fibroblasts was isolated from a pool of 3–4 lungs, as previously described (42). The isolated fibroblasts were then cultured in DMEM supplemented with 10% heat-inactivated fetal bovine serum (FBS, MP Biomedicals), 2% penicillin-streptomycin, and L-glutamine (Gibco, ThermoFisher Scientific).

In Vitro Stimulation With eCIRP and TGF- β 1

At passages 3–6, the cultured medium was replaced with reduced serum media Opti-MEM. After incubation overnight in Opti-MEM, the pulmonary fibroblasts were treated with phosphate-buffered saline (PBS), 1 μ g/mL recombinant mouse (rm) CIRP, 2 ng/mL rmTGF- β 1 (R&D Systems), or rmCIRP plus rmTGF- β 1. The rmCIRP was produced in our lab, as previously described (1). The cell lysates collected at 24 hours were used for high throughput mRNA sequencing and real-time reverse transcription-polymerase chain reaction (RT-PCR), the cell lysates collected at 48 hours were used for Western blotting (WB). Supernatants were collected at 48 hours and used for enzyme-linked immunosorbent assay (ELISA) quantification.

Isolation of the mRNA, RNA-Seq, and Analysis

RNA was isolated using Ambion's mirVana kit (catalog #AM1561, Thermo Fisher) following the manufacturer's recommendations and quantified on a Nanodrop 2000 (catalog # ND-2000, Thermo Fisher). All samples had 260/280 and 260/230 ratios between 1.8 and 2.1. RNA quality was further assessed with an RNA Nano Chip using a Bioanalyzer 2100 (Agilent). All samples had a RIN number of 8 or higher. RNA was stored at -80 until Library preparation. Libraries were prepared using Illumina TruSeq Stranded Total RNA Library Prep Kit (catalog # RS-122-2203, Illumina Inc). The mRNA expression was obtained by RNA-Seq libraries run on NextSeq 550 following the manufacturer's instructions. FastQC was used to ensure there was no adapter contamination and reads had acceptable quality scores (43). Sequenced segment alignments were performed using STAR2 (44) to the mouse GENCODE reference (45). The mRNA sequencing raw counts were obtained using ht-seq counts (46).

MA Plots, Principal Component, Pathways, and Time Series Analysis

After high-throughput mRNA sequencing raw counts were obtained, the data were analyzed and normalized using the DESeq2 standard workflow (47). M (log ratio) and A (mean average) (MA) plots were obtained using the function *plotMA*, to visually represent the differences between PBS and rmCIRP-treated cells by transforming the data onto logarithmic of base 2 (\log_2) fold changes vs. mean normalized count. The mRNA normalized counts were obtained using *plotCounts* function, which normalizes counts by sequencing depth. Principal component analysis was performed after variance stabilizing transformation (using *vst* function) to deal with the sampling variability of low counts and included correction for size factor (48). The pathway and time series analysis was done using the *Goexpress* workflow (49). The gene ontologies (GO) were first scored and ranked using the *GO_analyse* function, which consists of a random forest analysis to evaluate the ability of each gene to cluster samples according to the treatment groups in each analysis: pulmonary fibroblast mRNA sequencing data, PBS, eCIRP, TGF- β 1, or eCIRP+TGF- β 1; GSE132869 mRNA

sequencing data, PBS, or bleomycin. The heatmap for each GO was created using the *heatmap_GO* function and Z-scores were scaled on each gene included in GO. Time-series data were analyzed using the *expression_plot* function, which plots the expression profile of a specific gene smoothed across time points (days 7, 14, 21, 28, and 42) while representing the mean and confidence interval of groups of lung tissue samples (bleomycin and PBS injected groups).

Protein Detection and Quantification

For Western blotting, the cultured WT and TLR4^{-/-} primary pulmonary fibroblasts cells were scraped from 6 well culture plates and homogenized in a radioimmunoprecipitation assay buffer (RIPA) buffer containing phenylmethylsulfonyl fluoride (PMSF), Na-orthovanadate, and protease inhibitors. After centrifugation of cell lysates at 4°C and 12,000 rpm for 15 min, the total protein concentration was measured. The 10 µg protein of each sample was run in NuPAGE™ 4–12% Bis-Tris Gel (Invitrogen, Thermo Fisher Scientific), and gels were transferred to a nitrocellulose membrane. Membranes were blocked with 0.1% casein 1h at the room temperature, after that, they were incubated with primary antibodies such as CIRP (catalog # 10209-2-AP, Protein Tech), β-actin (clone AC-15, catalog # A5441, MilliporeSigma), tumor necrosis factor (TNF-α, catalog # 3707S, Cell Signalling Technology) and interleukin 1β (IL-1β, catalog #16806-1-AP, Protein Tech), MD2 (catalog # B100-56655, Novus Biologicals) and glyceraldehyde 3-phosphate dehydrogenase (GAPDH, catalog # 60004-1-Ig, Proteintech) at 4°C overnight. After washing the membranes with Tris-Buffered Saline (TBS) containing 0.1% Tween-20 (TBST), and TBS; they were incubated with secondary antibodies for 1 h at room temperature. The signal of protein bands was detected and measured by using Odyssey CLx Imaging Machine and Image Studio Ver 5.2 Software. The bands were normalized with GAPDH. For ELISA, the levels of IL-6 of cell culture supernatant were measured using the mouse IL-16 DuoSet ELISA kit (DY206, R&D Systems), and it was performed according to the company's protocol.

Isolation and Analysis of RT-PCR

Total RNA was isolated using Trizol reagent (Invitrogen) and reverse transcribed to cDNA using M-MLV (Moloney murine leukemia virus) reverse transcriptase (Applied Biosystems, Foster City, CA). Polymerase chain reactions (PCR) were carried out in a final volume of 10.5 µl, which included a 5 µl SYBR Green PCR master mix (Applied Biosystems) and 31 nM of both reverse and forward primers. GAPDH mRNA was used to normalize the amplification data, and fold changes were calculated in comparison with WT Control mice using the 2^{-(ΔΔCt)} method. The sequence of forward and reverse primers used were as follows:

GAPDH: 5'-CATCACTGCCACCCAGAAGACTG-3' (forward) and 5'-ATGCCAGTGAGCTTCCCGTTCAG-3'(reverse);
 TNF-α: 5'-AGACCCTCACACTCAGATCATCTTC-3' (forward) and 5'-TTGCTACGACGTGGGCTACA-3' (reverse);

IL-1β: 5'-CAGGATGAGGACATGAGCACC-3' (forward) and 5'-CTCTGCAGACTCAAACCTCCAC-3'(reverse);

IL-6: 5'-CCGGAGAGGAGACTTCACAG-3' (forward) and 5'-GGAAATTGGGGTAGGAAGGA-3'(reverse);

MD2 (Ly96): 5'-CGCTGCTTTCTCCCATATTGA-3' (forward) and 5'-CCTCAGTCTTATGCAGGGTTCA-3'(reverse).

Analysis of Gene Expression Omnibus Dataset

The expression datasets were obtained directly from the gene expression omnibus website (<https://www.ncbi.nlm.nih.gov/geo>) using the *getGEO* function of R (<http://www.r-project.org/>) 4.0.3 library called *GEOquery* (50). After obtaining the dataset for GSE132869, the columns from lung tissues were selected. This GEO contains RNA sequenced from lung tissues of mice injected with bleomycin (10 µg/g/day, 100 µl of 1 mg/ml solution per injection of a ~20 g mouse) or PBS five times per week for two weeks. The tissues were collected on 7, 14, 21, 28, and 42 days after the first injection (51). While the exact timing of peak inflammation and fibrosis in the lung, in this model, is not clear, based on previous studies, inflammation occurs between days 7 and 14, and peak fibrosis likely happens between days 21 and 28 (52–54). Day 14, which we call the inflammatory-to-fibrotic transition phase of exposure to bleomycin, is a time when both processes are active.

Statistical Analysis

Data from mRNA sequencing normalized count were analyzed using the results function of DESeq2 workflow, which estimates the log₂ fold change of maximum likelihood estimates (MLE) between treated and untreated samples per unit of change on the specific genes, and p-values provided are Benjamini-Hochberg (BH)-adjusted p-values with false discovery cut-off set to 0.1 (55). The p-values are set to 0 if they are too small to be represented (the smallest floating-point value to be represented in R is 2.225074e-308). Data for RT-PCR, WB, and ELISA are shown in the bar graphs as mean and standard deviation (SD), with individual values depicted by colored points. The comparisons were performed using two-way analysis of variance (ANOVA) followed by Tukey's multiple comparison test with the factors of two-way ANOVA being TLR4 gene expression status (WT vs. TLR4^{-/-}) and fibroblast treatment (PBS vs. CIRP). The groups were checked for Shapiro-Wilk test for normality prior to the application of two-way ANOVA.

RESULTS

eCIRP Induces Proinflammatory Cytokines in Pulmonary Fibroblasts via TLR4

To examine the effects of eCIRP on the expression of proinflammatory cytokines, we examined the normalized mRNA count (RNA-Seq), RT-PCR expression, and supernatant protein levels of TNF-α, IL-1β, and IL-6 in pulmonary fibroblasts isolated from the lungs of WT and TLR4^{-/-} mice and cultured for 24h with rmCIRP or PBS. Compared with PBS, rmCIRP significantly

increased the number of the mRNA normalized counts of TNF- α by 4.9 log₂ fold (adjusted p-value \approx 0, **Figure 1A**), IL-1 β by 9.9 log₂ fold (adjusted p-value \approx 0, **Figure 1D**), and IL-6 by 2.1 log₂ fold (adjusted p-value = 2.31e-33, **Figure 1G**). However, there were no significant increases in the mRNA normalized counts of TNF- α , IL-1 β , and IL-6 in TLR4^{-/-} cells stimulated with rmCIRP as compared to PBS (**Figures 1A, D, G**; for more details, please refer to **Supplementary Table 1**). We confirmed the RNA-Seq results

using RT-PCR amplification of mRNA obtained from a separate set of cells. Compared with PBS, rmCIRP significantly induced the WT fibroblast RT-PCR expression of TNF- α (23.6 fold, p<0.0001, **Figure 1B**), IL-1 β (3368.7 fold, p= 0.0002, **Figure 1E**), and IL-6 (14.0 fold, p<0.0001, **Figure 1H**) expression by rmCIRP. The mRNA levels of TNF- α , IL-1 β , and IL-6 measured by RT-PCR in TLR4^{-/-} pulmonary fibroblasts stimulated with rmCIRP, however, were significantly lower than those of WT stimulated with rmCIRP

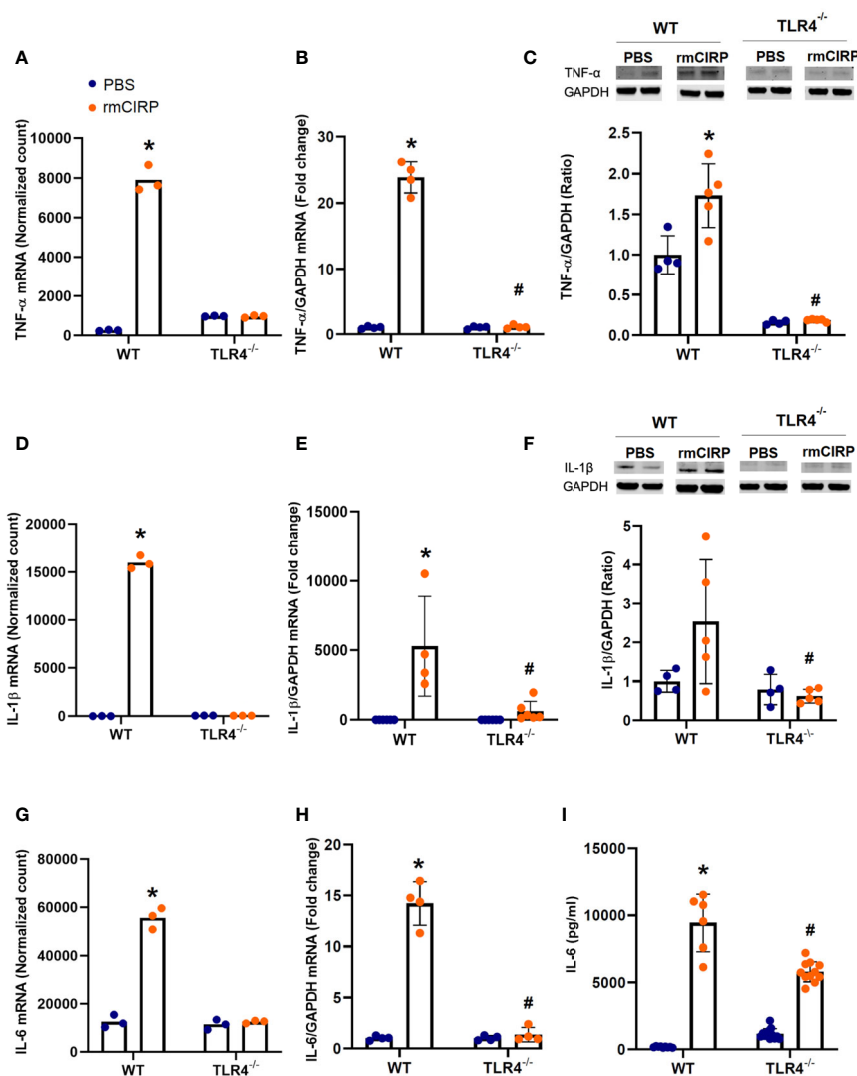


FIGURE 1 | eCIRP induces proinflammatory cytokines in pulmonary fibroblasts in a TLR4-dependent manner. Differential mRNA expression normalized counts for TNF- α (**A**), IL-1 β (**D**), and IL-6 (**G**) in pulmonary fibroblasts isolated from wild type (WT) and TLR4^{-/-} treated with PBS and 1 μ g/ml CIRP. Real-time reverse transcription-polymerase chain reaction (RT-PCR) for TNF- α (**B**), IL-6 (**E**), and (**G**) normalized against Glyceraldehyde 3-phosphate dehydrogenase (GAPDH) mRNA. Western blot (WB) analyses of TNF- α (**C**) and IL-1 β (**F**), and enzyme-linked immunosorbent assay (ELISA) analysis of IL-6 (**I**) in WT and TLR4^{-/-} pulmonary fibroblasts treated with PBS and 1 μ g/ml CIRP. Analyses for (**A, D, G**) are performed by log₂ fold change of maximum likelihood estimates (MLE) using the DESeq2 workflow and the p-values were adjusted by Benjamini-Hochberg (BH) with a false discovery cut-off set to 0.1. Analyses for (**E, F, H, I**) were done using two-way ANOVA with one factor being genetics (WT vs TLR4^{-/-}) and one factor being treatment (PBS vs. CIRP). *p<0.05 vs. WT PBS. #p<0.05 vs. WT CIRP. The groups were checked for Shapiro-Wilk test for normality prior to the application of two-way ANOVA. The mRNA sequencing (3 samples per group, 3 repeats per sample) and RT-PCR (4 samples per group, 2 repeats per sample) were done after the cells were incubated for 24 hours. The WBs (4-5 samples per group) and ELISA (6-12 samples per group, triplicate) were performed when cells were incubated for 48 hours. Representative samples for each lineage (WT vs. TLR4^{-/-}) are from a single blot shown for western blot analyses.

(**Figures 1B, E, H**). We also measured the effects of stimulation with rmCIRP on the pulmonary fibroblast protein expression of the above-mentioned cytokines (TNF- α and IL-1 β by WB, IL-6 by ELISA). Compared with PBS, rmCIRP significantly induced the WT fibroblast protein expression of TNF- α (1.7 fold, $p=0.0021$, **Figure 1C**) and IL-6 (53.4 fold, $p<0.0001$, **Figure 1I**) expression by rmCIRP. The protein levels of TNF- α and IL-6 in TLR4^{-/-} pulmonary fibroblasts stimulated with rmCIRP, however, were significantly lower than those of WT stimulated with rmCIRP (**Figures 1C, I**). Stimulation with rmCIRP increased the protein expression of IL-1 β in WT pulmonary fibroblasts by 2.5 fold, which showed a trend towards statistical significance ($p=0.0884$, **Figure 1F**). However, the protein expression of IL-1 β in rmCIRP-stimulated TLR4^{-/-} pulmonary fibroblasts was 75% lower than that of rmCIRP-stimulated WT cells ($p=0.0191$, **Figure 1F**). Taken together, these results indicate that eCIRP induces proinflammatory cytokines in pulmonary fibroblasts in a TLR4 dependent manner.

eCIRP Differentially Enriches TLR4 and its Dependent Pathways in Pulmonary Fibroblasts

eCIRP binds to and activates TLR4 (1). To determine the importance of TLR4 in eCIRP's induction of proinflammatory pulmonary fibroblasts, we examined the MA plots of genomic data from high throughput sequencing of mRNA data in WT

and TLR4^{-/-} pulmonary fibroblasts. Our analysis showed that the eCIRP-induced translational profile was restricted to WT pulmonary fibroblasts and did not occur in TLR4^{-/-} pulmonary fibroblasts (**Figures 2A, B**). In order to determine the effects of rmCIRP on the TLR4 and its related pathways, we analyzed the enrichment for transcripts associated with the TLR4 (GO:0034142) and Myd88 (GO:0002755) signaling pathways in WT pulmonary fibroblasts treated with PBS, rmCIRP, rmTGF- β 1, or the combination of the rmCIRP and rmTGF- β 1. Our analysis showed that stimulation with rmCIRP was associated with differential enrichment for both GO:0034142 and GO:0002755 (p -values; GO:0034142, <0.0001 , **Figure 2C**; GO:0002755, 0.0007, **Figure 2D**), irrespective of the presence of TGF- β 1. These results indicate that eCIRP changes the translational profile of pulmonary fibroblasts *via* TLR4 and induces TLR4-dependent pathways, irrespective of TGF- β 1.

eCIRP Induces MD2 Expression in Pulmonary Fibroblasts in a TLR4 Dependent Manner

eCIRP also binds to MD2, which forms a complex with TLR4 (1). To examine the role of eCIRP in the induction of TLR4's accessory pathway through the MD2 receptor, we examined the RNASeq normalized mRNA count, RT-PCR mRNA expression, and protein expression of MD2 in pulmonary fibroblasts isolated from the lungs of WT and TLR4^{-/-} mice. Stimulation with rmCIRP significantly

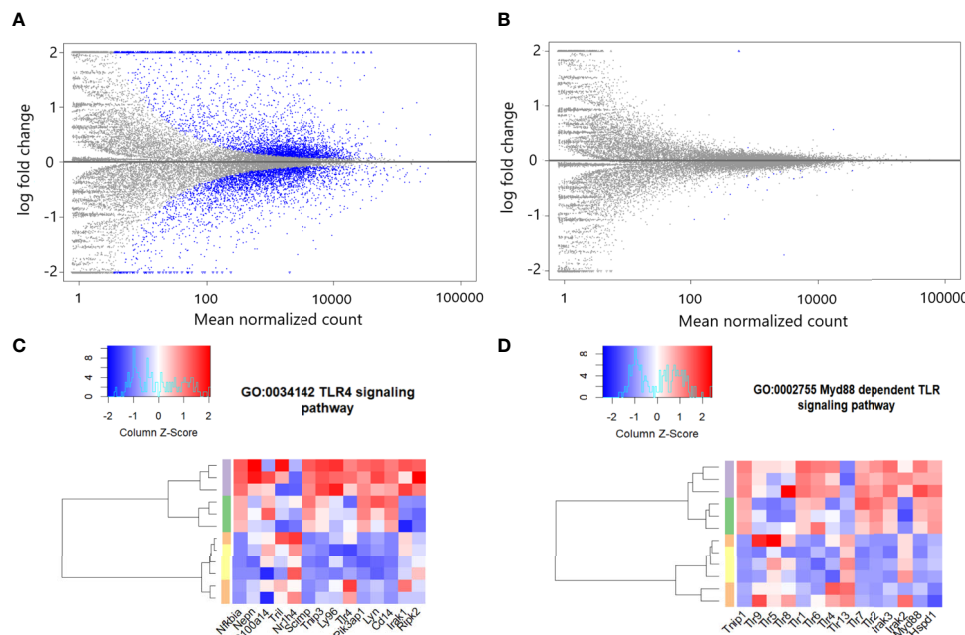


FIGURE 2 | eCIRP differentially enriches TLR4 and dependent pathways in pulmonary fibroblasts irrespective of TGF- β 1. MA plots for differential mRNA expression profile of 1 μ g/ml CIRP treatment vs. PBS treatment of pooled pulmonary fibroblasts isolated from wild type (WT) (**A**) and TLR4^{-/-} mice (**B**). Differential enrichment profile transcriptome of WT pulmonary fibroblasts isolated from mice and treated with PBS (orange), 2 ng/ml TGF- β 1 (yellow), 1 μ g/ml CIRP (purple), and the combination of the two (green) in gene ontologies 0034145 (toll-like receptor 4 signaling pathway) (**C**), 0002755 (MyD88-dependent toll-like receptor signaling pathway) (**D**) shown in heatmaps. The dendrogram clustering was made based on the hierarchical clustering of samples across all genes for each ontology profile. The heatmap color spectra were normalized across each gene. Z-score color key and histogram of counts presented in the left upper corner. Pulmonary fibroblasts were collected 24 hours after treatments described and prepared for RNA sequencing.

increased the MD2 mRNA normalized count in WT cells by 0.3 log₂ fold (adjusted $p=0.004$, **Figure 3A**). This induction, however, was not observed in the mRNA normalized count of TLR4^{-/-} cells (**Figure 3A**). Stimulation with rmCIRP also increased the mRNA expression of MD2 in WT pulmonary fibroblasts by 1.9 fold ($p=0.047$), but a similar increase was not seen in TLR4^{-/-} pulmonary fibroblasts (**Figure 3B**). Although there was an increase in protein expression of MD-2 in WT pulmonary fibroblasts treated with eCIRP, the increase was not statistically significant. Conversely, the MD2 protein expression of TLR4^{-/-} pulmonary fibroblasts stimulated with rmCIRP was significantly lower than that of WT pulmonary fibroblasts stimulated with rmCIRP ($p=0.3741$, **Figure 3C**). These data suggest that eCIRP induces MD2 expression in pulmonary fibroblasts in a TLR4 dependent manner.

eCIRP Induction of Proinflammatory Pulmonary Fibroblast Phenotype Is Not Dependent on TGF- β 1

In the previous section, we showed that TGF- β 1 did not significantly affect the transcriptional profile of TLR4 and Myd88 signaling pathways in WT pulmonary fibroblasts (**Figures 2C, D**). To determine whether eCIRP requires TGF- β 1 to induce the proinflammatory phenotype, we conducted a principal component (PC) analysis of mRNA profile sequenced from WT pulmonary fibroblasts treated with PBS, rmCIRP, rmTGF- β 1, and the combination of the rmCIRP and rmTGF- β 1. Our analysis showed that two PCs explain 95% of the variation in mRNA genomic data in WT pulmonary fibroblasts: PC1 explained 84% of the variance and PC2, 11%. Furthermore, the variance explained by PC1 aligned well with stimulation by rmCIRP, whereas PC2 aligned well with stimulation by TGF- β 1 (**Figure 4A**). We then examined selected genes to see the direction of contribution and observed that TNF- α , IL-1 α , IL-1 β , IL-6, and CxCl2 contributed to

the variance towards the eCIRP-aligned PC1. Furthermore, MD2 (Ly96) and Myd88 also contributed to the variance along PC1, albeit to a lesser degree (**Figure 4A**). To see the full list of genes examined, please see **Supplementary Figure 1**. Taken together, these results indicate that eCIRP induces a proinflammatory phenotype of pulmonary fibroblasts independently of TGF- β 1.

eCIRP Differentially Enriches Proinflammatory Transcriptional Profiles Irrespective of TGF- β 1

Stimulation with rmCIRP also caused a transcriptional reprogramming that was differentially enriched for genes associated with the TNF- α mediated signaling pathway (GO:0033209, p -value = 0.008, **Figure 5A**) and positive regulation of IL-6 production (GO:00032755, p -value <0.0001, **Figure 5B**) in WT pulmonary fibroblasts stimulated with rmCIRP or the combination of the rmCIRP and rmTGF- β 1. However, differential enrichment for these two pathways was not present in the transcriptome of pulmonary fibroblasts cultured with rmTGF- β 1. To see high-resolution figures to examine genes involved in GOs analyzed, please see **Supplementary Figures 2, 3**. As such, eCIRP differentially enriches the proinflammatory transcriptional profile in pulmonary fibroblasts that includes TNF- α signaling and IL-6 production.

Proinflammatory Gene Profiles in Bleomycin Treated Lungs in the Inflammatory-To-Fibrotic Transition Phase Recapitulate Pulmonary Fibroblasts Stimulated With eCIRP

To compare the transcriptomic changes after stimulation with eCIRP with those in the lungs of mice exposed to bleomycin, we examined a publicly available Gene Expression Omnibus (GEO) profile (GSE132869) containing high throughput RNA sequences

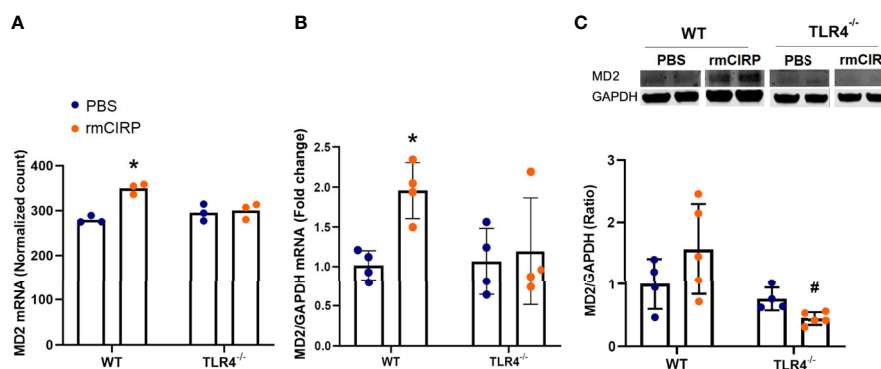


FIGURE 3 | eCIRP induces MD2 expression in pulmonary fibroblasts in a TLR4 dependent manner. Differential mRNA expression profile (**A**), real-time reverse transcription-polymerase chain reaction (RT-PCR) (**B**), and western blot (WB) analyses for MD2 in WT and TLR4^{-/-} pulmonary fibroblasts treated with PBS and 1 μ g/ml CIRP. Analysis for A was performed by log₂ fold change of maximum likelihood estimates (MLE) using the DESeq2 workflow and the p -values were adjusted by Benjamini-Hochberg (BH) with a false discovery cut-off set to 0.1. Analyses for (**B, C**) were done using two-way ANOVA with one factor being genetics (WT vs TLR4^{-/-}) and one factor being treatment (PBS vs. CIRP). * $p < 0.05$ vs. WT PBS. # $p < 0.05$ vs. WT CIRP. The groups were checked for Shapiro-Wilk test for normality prior to the application of two-way ANOVA. The mRNA sequencing (3 samples per group, 3 repeats per instance) and RT-PCR (4 samples per group, 2 repeats per instance) were done after the cells were incubated for 24 hours. The WBs (4-5 samples per group) were performed when cells were incubated for 48 hours. Representative samples for each lineage (WT vs. TLR4^{-/-}) are from a single blot shown for western blot analyses.

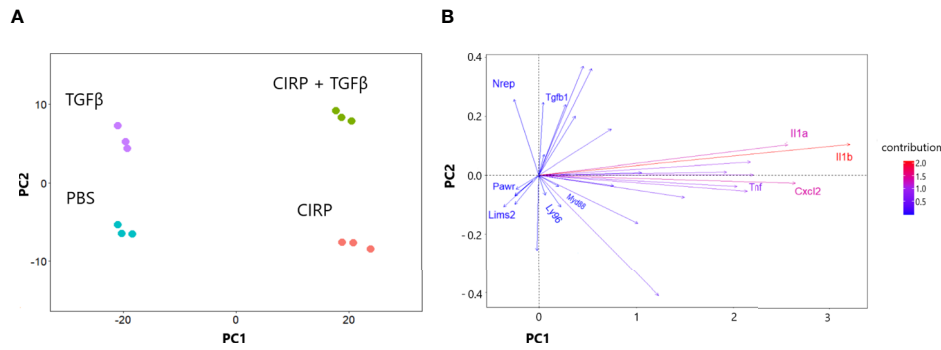


FIGURE 4 | eCIRP induction of proinflammatory phenotype is not dependent on TGF-β1. Principal component analysis (PCA) of the mRNA expression profile of WT pulmonary fibroblasts treated with PBS, 1 μg/ml CIRP, 2 ng/ml TGF-β1, and combination of the two shown in clustering of samples (A) and direction of selected proinflammatory/profibrotic genes (B). Pulmonary fibroblasts were collected 24 hours after treatments and prepared for RNA sequencing. PC1 and PC2 explained 84 and 11% of the variance, respectively. PC, Principal component.

from lung tissue of WT mice collected on days 7, 14, 21, 28, or 42 from the start of bleomycin injection. Similar to our observations in eCIRP-stimulated lung fibroblasts, the lung transcriptome on day 14 after bleomycin showed significant upregulation of TLR4, MD2, and Myd88 mRNA counts (Figures 6A, C, E). The lung transcriptome on day 14 was also differentially enriched for genes associated with the TLR signaling pathway (GO:0002224, p-value = 0.005, Figure 6B), TRIF dependent TLR signaling pathway (GO:0035666, p-value = 0.013, Figure 6D), and Myd88 dependent TLR signaling pathway (GO:0002755, p-value = 0.04, Figure 6F). To see a higher resolution of Figure 6B, please refer to Supplementary Figure 4. As a whole, the results indicate that the TLR4 and related genes and pathways activated by eCIRP in pulmonary fibroblasts are also transcriptionally active on day 14 after bleomycin injection.

To determine the timeline at which inflammatory cytokines and their cellular response pathways are induced, we examined the mRNA of cytokines TNF-α, IL-6, and the cellular response to these cytokines. Similar to our observations in eCIRP-stimulated lung fibroblasts, the lung transcriptome on day 14 after bleomycin showed significant upregulation of TNF-α and IL-6 mRNA counts (Figures 7A, C). The lung transcriptome on day 14 was also differentially enriched for genes associated with the cellular response to TNF-α (GO:0071356, p-value = 0.009, Figure 7B) and cellular response to IL-6 (GO:0071354, p-value = 0.021, Figure 7D). To see a higher resolution of Figure 7B, please refer to Supplementary Figure 5. Taken together, the results indicate that the TLR4 and related genes and pathways activated by eCIRP in pulmonary fibroblasts are also transcriptionally active on day 14 after bleomycin injection.

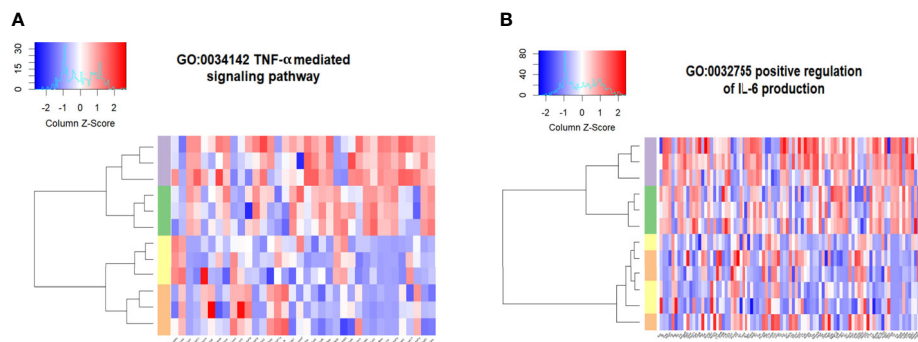


FIGURE 5 | eCIRP differentially enriches proinflammatory transcriptional profiles irrespective of TGF-β1. Differential enrichment profile of WT pulmonary fibroblasts isolated from mice and treated with PBS (orange), 2 ng/ml TGF-β1 (yellow), 1 μg/ml CIRP (purple), and the combination of the two (green) in gene ontologies 0033209 (TNF-α signaling pathway) (A) and 0032755 (positive regulation of IL-6 production) (B) shown in heatmaps. The dendrogram clustering was made based on the hierarchical clustering of samples across all genes for each ontology profile. The heatmap of the color spectra was normalized across each gene. Z-score color key and histogram of counts presented in the left upper corner. Pulmonary fibroblasts were collected 24 hours after treatments described and prepared for RNA sequencing.

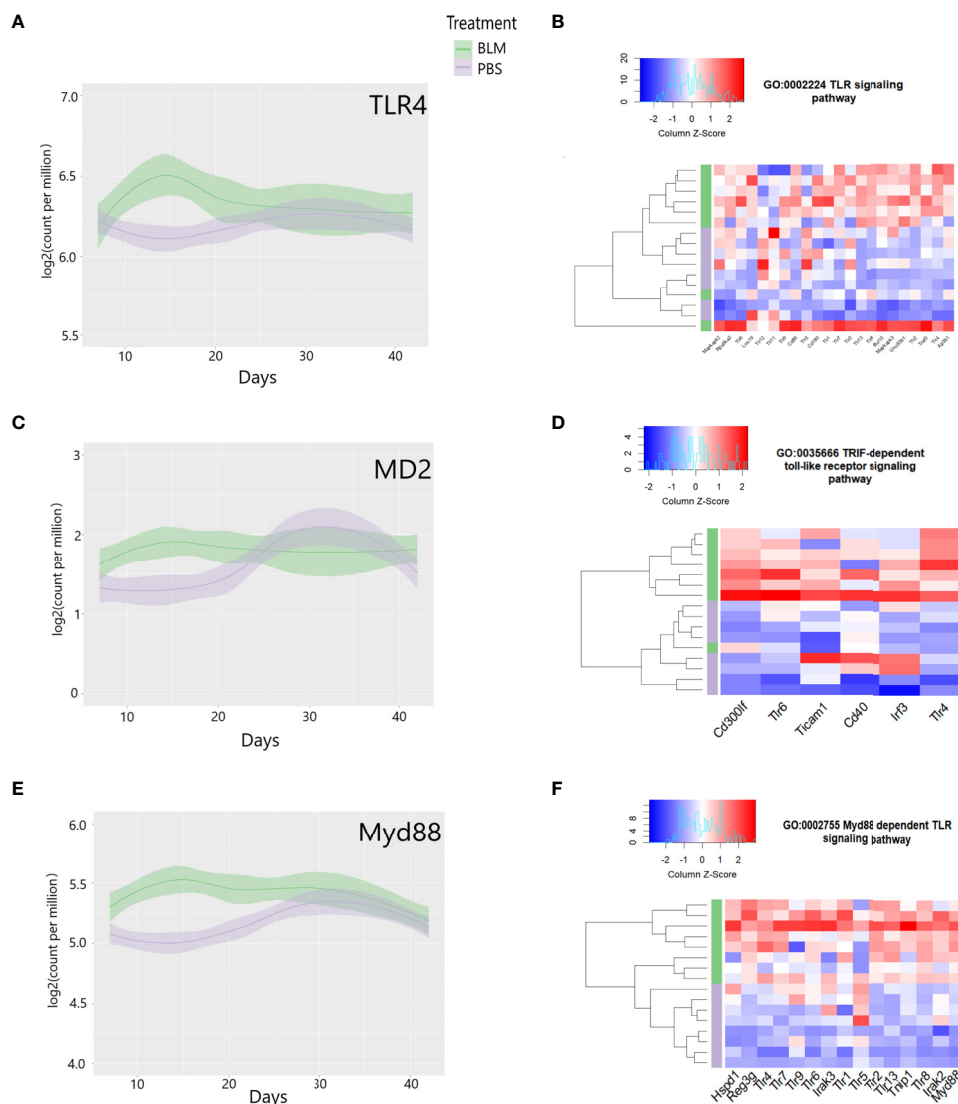


FIGURE 6 | Toll-like receptor 4 (TLR4) and related genes are induced, and pathways are differentially enriched on day 14 of bleomycin injection in lung tissue. Examinations of a publicly available gene expression omnibus (GEO) profile: GSE132869. Expression profiles of TLR4 (A), MD-2 (C), and Myd88 (E) mRNA as base 2 logarithmic counts per million over time (days) in lung tissue of mice with the means and 0.95 confidence intervals. The samples are presented as bleomycin injected group (in green), and PBS injected mice (in purple). The plots are smoothed using a generalized linear model. Differential enrichment profile of lung tissues of PBS injected (purple) and bleomycin injected mice on day 14 from the start of injections in gene ontologies 0002224 (toll-like receptor signaling pathway) (B), 0035666 (TRIF-dependent toll-like receptor signaling pathway) (D), and 0002755 (MyD88-dependent toll-like receptor signaling pathway) (F) shown in the heatmap. The dendrogram clustering was made based on the hierarchical clustering of samples across all genes for each ontology profile. The heatmap of the color spectra was normalized across each gene. Z-score color key and histogram of counts presented in the left upper corner. Female mice (~12 weeks old) subcutaneously injected daily either with bleomycin (10 mg/kg/day) or PBS. Injections began on Day 0 and were done five times per week for two weeks. Mice were sacrificed on days 7, 14, 21, 28, and 42, and the lung tissues were collected.

DISCUSSION

Fibroblasts are key cells involved in the fibrotic process (56). In order to illuminate the possible contribution of eCIRP to the fibrotic process, we investigated how eCIRP influences the transcriptional profile of the pulmonary fibroblasts. We evaluated the transcriptional response of lung fibroblasts stimulated with eCIRP with a particular focus on proinflammatory and TLR4-induced

pathways. We also evaluated how these pathways change over the course of bleomycin-induced pulmonary fibrosis. What we observed was that eCIRP amplifies proinflammatory cytokines in a TLR4 dependent manner and differentially enriches the inflammatory pathways. Furthermore, we found that this activation pattern recapitulates that of the inflammatory-to-fibrotic transition phase in the bleomycin-induced pulmonary fibrosis model.

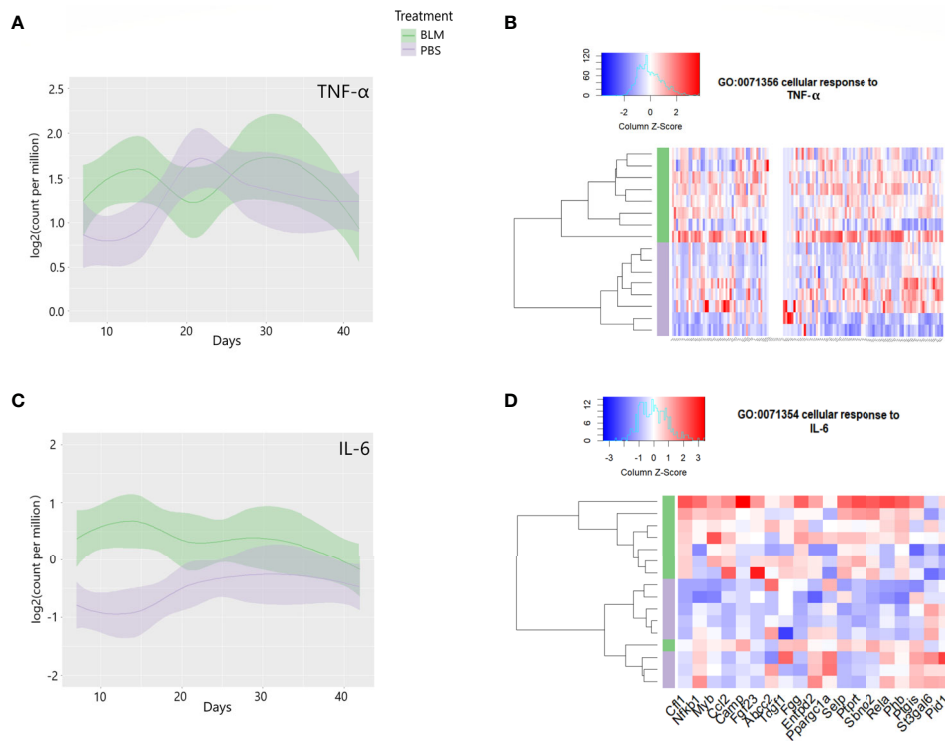


FIGURE 7 | Proinflammatory cytokines are induced, and their cellular responses are enriched on day 14 of bleomycin injection in lung tissue. Examinations of a publicly available gene expression omnibus (GEO) profile: GSE132869. Expression profiles of TNF- α (A) and IL-6 (C) mRNA as base 2 logarithmic counts per million over time (days) in lung tissue of mice with the means and 0.95 confidence intervals. The samples are presented as bleomycin injected group (in green), and PBS injected mice (in purple). The plots are smoothed using a generalized linear model. Differential enrichment profile of lung tissues of PBS injected (purple), and bleomycin injected mice on day 14 from the start of injections in gene ontologies 0071356 (cellular response to TNF- α , B) and 0071354 (cellular response to IL-6, D) shown in the heatmap. The dendrogram clustering was made based on the hierarchical clustering of samples across all genes for each ontology profile. The heatmap of the color spectra was normalized across each gene. Z-score color key and histogram of counts presented in the left upper corner. Female mice (~12 weeks old) subcutaneously injected daily either with bleomycin (10 mg/kg/day) or PBS. Injections began on Day 0 and were done five times per week for two weeks. Mice were sacrificed on days 7, 14, 21, 28, and 42, and the lung tissues were collected.

We have previously shown that CIRP binds with high affinity to the TLR4-MD2 complex, as well as to TLR4 and MD2 individually (1). Furthermore, TLR4 expression is known to be elevated in lung biopsies of patients with pulmonary fibrosis caused by chronic inflammatory diseases (21, 57, 58). While TGF- β 1 is required for profibrotic activation of the fibroblasts, this activation and induction of organ fibrosis require a primed cellular microenvironment, which can be induced by TLR4 activation (22, 59, 60). The role of inflammatory fibroblasts in the pathogenesis of fibrosis has been studied (36, 61, 62). Inflammatory fibroblasts persistently activate the fibroblasts in an autocrine/paracrine manner in the lungs, resulting in pulmonary fibrosis (63–65). The proinflammatory role of TLR4-MD2 complex and Myd88 signaling pathway in the lungs has also been evaluated (66–69) and associated with the fibrotic process leading to pulmonary fibrosis (60, 70–74). In our study, we found that eCIRP induces proinflammatory cytokines and their pathways in pulmonary fibroblasts in a TLR4 dependent manner. Furthermore, we showed that the TLR co-receptor MD2 and the downstream Myd88 pathway are enriched

by eCIRP in a TLR4 dependent manner. These results shed light on the mechanism by which eCIRP induces proinflammatory pulmonary fibroblasts during the inflammatory phase in the pathogenesis of bleomycin-induced pulmonary fibrosis.

It is well known that TGF- β 1 is the master regulator, and its signaling is required for the promotion and maintenance of the fibrotic process in the lungs (75–77). The recent works by Bhattacharyya et al. showed that TLR4 signaling synergizes with TGF- β in the activation of fibroblasts in the setting of pulmonary fibrosis (21, 78, 79). After illustrating that eCIRP proinflammatory programming of fibroblasts is done in a TLR4 dependent, we set out to see the effect of TGF- β in this process. Our principal component analysis showed that the principal component that explains the variation in inflammatory cytokines and chemokines aligns with the treatment of eCIRP and not TGF- β 1 (Figure 4 and Supplementary Figure 6). This confirms that the proinflammatory programming of fibroblasts is dependent on eCIRP, not TGF- β 1.

In order to establish how eCIRP's induction of proinflammatory phenotype may contribute to the pathogenesis of bleomycin-

induced pulmonary fibrosis, we examined the pathways induced by eCIRP in fibroblast in the lung tissues of mice. We showed that TLR4, MD2, Myd88, and related pathways are significantly induced in lungs collected on day 14 of bleomycin-induced pulmonary fibrosis. Proinflammatory cytokines and the related were also significantly overrepresented in day 14 of pulmonary fibrosis lung tissues, showing that the changes in the lung transcriptome during the inflammatory-to-fibrotic transition phase after bleomycin injection recapitulate those pulmonary fibroblasts stimulated with eCIRP. This is in line with previous studies showing an increase in the lung infiltration by total white blood cells, neutrophils, and macrophages peaks at day 14, the expressions of profibrotic markers peak at day 21–28 (53, 54, 80, 81). We have previously shown that eCIRP promotes acute lung injury *via* activation of macrophages, neutrophils, pneumocytes, and lung vascular endothelial cells in the contexts of sepsis, hemorrhagic shock, and intestinal ischemia/reperfusion injury (1, 5, 6, 82–84). However, little was known about eCIRP's role in chronic inflammatory diseases of the lung. Our results show that eCIRP activates a proinflammatory phenotype in pulmonary fibroblasts, illuminating a potential mechanism by which eCIRP in the lung environment in the setting of chronic inflammation plays a critical priming role leading to lung fibrosis.

Our results should be interpreted taking into consideration some particularities and limitations. Our RNASeq analysis focused on TLR4 and proinflammatory genes, not on other high-ranking but unrelated genes and pathways. Our study was underpowered to detect changes of small magnitude and high variance. We did not perform a time-course analysis in our *in vitro* experiments, which might further show how fibroblast transcription can fluctuate and change over time, as other sequencing analyses have demonstrated (85–87). In our *in vivo* time series analysis, while we were able to measure total CIRP levels in pulmonary tissues and show it is elevated prior to day 14 (**Supplementary Figure 7**), we were not able to measure the levels of eCIRP in the lung interstitial space, which would further clarify the link between eCIRP and pulmonary fibrosis. This model only considered the subcutaneous bleomycin-induced pulmonary fibrosis, which models global inflammatory diseases that cause interstitial lung fibrosis (52, 60, 88, 89). The study of other models can shed light on the role of DAMPs such as eCIRP on other pulmonary diseases causing lung fibrosis.

In summary, we showed that eCIRP induces an inflammatory phenotype in pulmonary fibroblasts, which recapitulates that of lung tissue during the inflammatory phase of bleomycin-induced pulmonary fibrosis. Our results not only shed light on the mechanism by which eCIRP promotes inflammatory pulmonary fibroblasts but also show a possible stage at which

this phenotype contributes to the most commonly used pre-clinical model of pulmonary fibrosis. Our study suggests that eCIRP is critical for the proinflammatory fibroblasts reprogramming and may represent a druggable target to stop the progression of pulmonary fibrosis in chronic inflammatory diseases affecting the lung.

DATA AVAILABILITY STATEMENT

The data has been uploaded to NCBI - accession number GSE178255 ([https://www.ncbi.nlm.nih.gov/gds/?term=GSE178255\[Accession\]](https://www.ncbi.nlm.nih.gov/gds/?term=GSE178255[Accession])).

ETHICS STATEMENT

The animal study was reviewed and approved by Feinstein Institute's IACUC.

AUTHOR CONTRIBUTIONS

SB, MB, and PW designed the experiments. SB and ES performed all experiments and analyzed the data. MB and PW critically reviewed the manuscript. MB and PW conceived the idea and supervised the project. All authors contributed to the article and approved the submitted version.

FUNDING

This study was supported by the National Institutes of Health (NIH) grants R01HL076179 and R35GM118337 (PW).

ACKNOWLEDGMENTS

We would like to thank Monowar Aziz, PhD for valuable discussions and assistance.

SUPPLEMENTARY MATERIAL

The Supplementary Material for this article can be found online at: <https://www.frontiersin.org/articles/10.3389/fimmu.2021.721970/full#supplementary-material>

REFERENCES

1. Qiang X, Yang W-L, Wu R, Zhou M, Jacob A, Dong W, et al. Cold-Inducible RNA-binding Protein (CIRP) Triggers Inflammatory Responses in Hemorrhagic Shock and Sepsis. *Nat Med* (2013) 19:1489–95. doi: 10.1038/nm.3368
2. Zhang F, Brenner M, Yang W-L, Wang P. A Cold-Inducible RNA-binding Protein (CIRP)-Derived Peptide Attenuates Inflammation and Organ Injury in Septic Mice. *Sci Rep* (2018) 8:3052. doi: 10.1038/s41598-017-13139-z
3. Cen C, Yang W-L, Yen H-T, Nicastro JM, Coppa GF, Wang P. Deficiency of Cold-Inducible Ribonucleic Acid-Binding Protein Reduces Renal Injury After Ischemia-Reperfusion. *Surgery* (2016) 160:473–83. doi: 10.1016/j.surg.2016.04.014
4. Jacob A, Ma Y, Nasiri E, Ochani M, Carrion J, Peng S, et al. Extracellular Cold Inducible RNA-binding Protein Mediates Binge Alcohol-Induced Brain Hypoactivity and Impaired Cognition in Mice. *Mol Med* (2019) 25:24. doi: 10.1186/s10020-019-0092-3
5. Cen C, McGinn J, Aziz M, Yang W-L, Cagliani J, Nicastro JM, et al. Deficiency in Cold-Inducible RNA-binding Protein Attenuates Acute Respiratory

- Distress Syndrome Induced by Intestinal Ischemia-Reperfusion. *Surgery* (2017) 162:917–27. doi: 10.1016/j.surg.2017.06.004
6. Aziz M, Brenner M, Wang P. Extracellular CIRP (eCIRP) and Inflammation. *J Leukoc Biol* (2019) 106:133–46. doi: 10.1002/JLB.3MIR1118-443R
 7. Tan C, Gurien SD, Royster W, Aziz M, Wang P. Extracellular CIRP Induces Inflammation in Alveolar Type II Cells Via TREM-1. *Front Cell Dev Biol* (2020) 8:579157. doi: 10.3389/fcell.2020.579157
 8. Gurien SD, Aziz M, Jin H, Wang H, He M, Al-Abed Y, et al. Extracellular microRNA 130b-3p Inhibits eCIRP-induced Inflammation. *EMBO Rep* (2020) 21:e48075. doi: 10.15252/embr.201948075
 9. Yang W-L, Sharma A, Wang Z, Li Z, Fan J, Wang P. Cold-Inducible RNA-binding Protein Causes Endothelial Dysfunction Via Activation of Nlrp3 Inflammasome. *Sci Rep* (2016) 6:26571. doi: 10.1038/srep26571
 10. Hamada N, Maeyama T, Kawaguchi T, Yoshimi M, Fukumoto J, Yamada M, et al. The Role of High Mobility Group Box1 in Pulmonary Fibrosis. *Am J Respir Cell Mol Biol* (2008) 39:440–7. doi: 10.1165/rcmb.2007-0330OC
 11. Bellaye P-S, Wettstein G, Burgy O, Besnard V, Joannes A, Colas J, et al. The Small Heat-Shock Protein α -Crystallin Is Essential for the Nuclear Localization of Smad4: Impact on Pulmonary Fibrosis. *J Pathol* (2014) 232:458–72. doi: 10.1002/path.4314
 12. Akiyama N, Hozumi H, Isayama T, Okada J, Sugiura K, Yasui H, et al. Clinical Significance of Serum S100 Calcium-Binding Protein A4 in Idiopathic Pulmonary Fibrosis. *Respirology* (2020) 25:743–9. doi: 10.1111/resp.13707
 13. Herath TDK, Darveau RP, Seneviratne CJ, Wang C-Y, Wang Y, Jin L. Tetra- and Penta-Acylated Lipid A Structures of Porphyromonas Gingivalis LPS Differentially Activate TLR4-mediated NF-kb Signal Transduction Cascade and Immuno-Inflammatory Response in Human Gingival Fibroblasts. *PLoS One* (2013) 8:e58496. doi: 10.1371/journal.pone.0058496
 14. Müller H-DH-D, Cvikl BB, Lussi AA, Gruber RR. Salivary Pellets Induce a Pro-Inflammatory Response Involving the TLR4-NF-kb Pathway in Gingival Fibroblasts. *BMC Oral Health* (2016) 17:15. doi: 10.1186/s12903-016-0229-5
 15. Li K, Lv G, Pan L, Sirt1 Alleviates LPS Induced Inflammation of Periodontal Ligament Fibroblasts Via Downregulation of TLR4. *Int J Biol Macromol* (2018) 119:249–54. doi: 10.1016/j.ijbiomac.2018.07.099
 16. Jian C-X, Li M-Z, Zheng W-Y, He Y, Ren Y, Wu Z-M, et al. Tormentone Acid Inhibits LPS-induced Inflammatory Response in Human Gingival Fibroblasts Via Inhibition of TLR4-mediated NF-kb and MAPK Signaling Pathway. *Arch Oral Biol* (2015) 60:1327–32. doi: 10.1016/j.archoralbio.2015.05.005
 17. Fineschi S, Goffin L, Rezzonico R, Cozzi F, Dayer J-M, Meroni PL, et al. Antifibroblast Antibodies in Systemic Sclerosis Induce Fibroblasts to Produce Proinflammatory Chemokines, With Partial Exploitation of Toll-Like Receptor 4. *Arthritis Rheum* (2008) 58:3913–23. doi: 10.1002/art.24049
 18. Meng X-M, Nikolic-Paterson DJ, Lan HY. Tgf- β : The Master Regulator of Fibrosis. *Nat Rev Nephrol* (2016) 12:325–38. doi: 10.1038/nrneph.2016.48
 19. Iyer SN, Gurujeyalakshmi G, Giri SN. Effects of Pirfenidone on Transforming Growth Factor-Beta Gene Expression at the Transcriptional Level in Bleomycin Hamster Model of Lung Fibrosis. *J Pharmacol Exp Ther* (1999) 291:367–73.
 20. Miyazawa K, Miyazono K. Regulation of TGF- β Family Signaling by Inhibitory Smads. *Cold Spring Harb Perspect Biol* (2017) 9:a022095. doi: 10.1101/cshperspect.a022095
 21. Bhattacharyya S, Kelley K, Melichian DS, Tamaki Z, Fang F, Su Y, et al. Toll-Like Receptor 4 Signaling Augments Transforming Growth Factor- β Responses: A Novel Mechanism for Maintaining and Amplifying Fibrosis in Scleroderma. *Am J Pathol* (2013) 182:192–205. doi: 10.1016/j.ajpath.2012.09.007
 22. Seki E, De Minicis S, Osterreicher CH, Kluwe J, Osawa Y, Brenner DA, et al. TLR4 Enhances TGF-beta Signaling and Hepatic Fibrosis. *Nat Med* (2007) 13:1324–32. doi: 10.1038/nm1663
 23. Derynck R, Muthusamy BP, Saeteurn KY. Signaling Pathway Cooperation in TGF- β -Induced Epithelial-Mesenchymal Transition. *Curr Opin Cell Biol* (2014) 31:56–66. doi: 10.1016/j.ccb.2014.09.001
 24. Epstein Shochet G, Brook E, Bardenstein-Wald B, Shitrit D. Tgf- β Pathway Activation by Idiopathic Pulmonary Fibrosis (IPF) Fibroblast Derived Soluble Factors is Mediated by IL-6 Trans-Signaling. *Respir Res* (2020) 21:56. doi: 10.1186/s12931-020-1319-0
 25. Hou J, Ma T, Cao H, Chen Y, Wang C, Chen X, et al. Tnf- α -Induced NF-kb Activation Promotes Myofibroblast Differentiation of LR-MSCs and Exacerbates Bleomycin-Induced Pulmonary Fibrosis. *J Cell Physiol* (2018) 233:2409–19. doi: 10.1002/jcp.26112
 26. Kach J, Sandbo N, Born W, Brain S, Dulin N. Regulation of Pulmonary Myofibroblast Differentiation and Bleomycin Induced Pulmonary Fibrosis by Adrenomedullin. *Am J Physiol Lung Cell Mol Physiol* (2012) 304(11):L757–64. doi: 10.1164/ajrccm-conference.2012.185.1_meetingabstracts.a5535
 27. Sieber P, Schäfer A, Lieberherr R, Le Goff F, Stritt M, Welford RWD, et al. Novel High-Throughput Myofibroblast Assays Identify Agonists With Therapeutic Potential in Pulmonary Fibrosis That Act Via EP2 and EP4 Receptors. *PLoS One* (2018) 13:e0207872. doi: 10.1371/journal.pone.0207872
 28. Jiang D, Dey T, Liu G. Recent Developments in the Pathobiology of Lung Myofibroblasts. *Expert Rev Respir Med* (2021) 15:239–47. doi: 10.1080/17476348.2021.1829972
 29. Wang C, Cao H, Gu S, Shi C, Chen X, Han X. Expression Analysis of microRNAs and mRNAs in Myofibroblast Differentiation of Lung Resident Mesenchymal Stem Cells. *Differentiation* (2020) 112:10–6. doi: 10.1016/j.diff.2019.11.002
 30. Lim H, Moon A. Inflammatory Fibroblasts in Cancer. *Arch Pharmacol Res* (2016) 39:1021–31. doi: 10.1007/s12272-016-0787-8
 31. Mizoguchi F, Slowikowski K, Wei K, Marshall JL, Rao DA, Chang SK, et al. Functionally Distinct Disease-Associated Fibroblast Subsets in Rheumatoid Arthritis. *Nat Commun* (2018) 9:789. doi: 10.1038/s41467-018-02892-y
 32. Frangogiannis NG. Fibroblast-Extracellular Matrix Interactions in Tissue Fibrosis. *Curr Pathobiol Rep* (2016) 4:11–8. doi: 10.1007/s40139-016-0099-1
 33. Bozkurt SB, Hakki SS, Hakki EE, Durak U, Kantarci A. Porphyromonas Gingivalis Lipopolysaccharide Induces a Pro-Inflammatory Human Gingival Fibroblast Phenotype. *Inflammation* (2017) 40:144–53. doi: 10.1007/s10753-016-0463-7
 34. Bolívar A, Anfossi R, Humeres C, Vivar R, Boza P, Muñoz C, et al. Ifn- β Plays Both Pro- and Anti-Inflammatory Roles in the Rat Cardiac Fibroblast Through Differential STAT Protein Activation. *Front Pharmacol* (2018) 9:1368. doi: 10.3389/fphar.2018.01368
 35. Gómez-Ochoa I, Gómez-Ochoa P, Gómez-Casal F, Catiuela E, Larrad-Mur L. Pulsed Electromagnetic Fields Decrease Proinflammatory Cytokine Secretion (IL-1 β and TNF- α) on Human Fibroblast-Like Cell Culture. *Rheumatol Int* (2011) 31:1283–9. doi: 10.1007/s00296-010-1488-0
 36. Chizzolini C, Raschi E, Rezzonico R, Testoni C, Mallone R, Gabrielli A, et al. Autoantibodies to Fibroblasts Induce a Proadhesive and Proinflammatory Fibroblast Phenotype in Patients With Systemic Sclerosis. *Arthritis Rheum* (2002) 46:1602–13. doi: 10.1002/art.10361
 37. Schanstra JP, Bataillé E, Marin Castaño ME, Barascud Y, Hirtz C, Pesquero JB, et al. The B1-agonist [des-Arg10]-kallidin Activates Transcription Factor NF-kappaB and Induces Homologous Upregulation of the Bradykinin B1-receptor in Cultured Human Lung Fibroblasts. *J Clin Invest* (1998) 101:2080–91. doi: 10.1172/JCI1359
 38. Coil J, Tam E, Waterfield JD. Proinflammatory Cytokine Profiles in Pulp Fibroblasts Stimulated With Lipopolysaccharide and Methyl Mercaptan. *J Endod* (2004) 30:88–91. doi: 10.1097/00004770-200402000-00006
 39. Wendell KJ, Stein SH. Regulation of Cytokine Production in Human Gingival Fibroblasts Following Treatment With Nicotine and Lipopolysaccharide. *J Periodontol* (2001) 72:1038–44. doi: 10.1902/jop.2001.72.8.1038
 40. Saxena A, Chen W, Su Y, Rai V, Uche OU, Li N, et al. IL-1 Induces Proinflammatory Leukocyte Infiltration and Regulates Fibroblast Phenotype in the Infarcted Myocardium. *J Immunol* (2013) 191:4838–48. doi: 10.4049/jimmunol.1300725
 41. Petrie WK, Wallace SL. *The Care and Feeding of an IACUC: The Organization and Management of an Institutional Animal Care and Use Committee*. 2nd ed. CRC Press (2015).
 42. Seluanov A, Vaidya A, Gorbunova V. Establishing Primary Adult Fibroblast Cultures From Rodents. *J Vis Exp* (2010) (44):4033. doi: 10.3791/2033
 43. Andrews S. *Babraham Bioinformatics - Fastqc A Quality Control Tool for High Throughput Sequence Data*. Available at: <http://www.bioinformatics.babraham.ac.uk/projects/fastqc/> (Accessed March 17, 2021).
 44. Dobin A, Gingeras TR. Optimizing RNA-Seq Mapping With STAR. *Methods Mol Biol* (2016) 1415:245–62. doi: 10.1007/978-1-4939-3572-7_13
 45. Frankish A, Diekhans M, Ferreira A-M, Johnson R, Jungreis I, Loveland J, et al. GENCODE Reference Annotation for the Human and Mouse Genomes. *Nucleic Acids Res* (2019) 47:D766–73. doi: 10.1093/nar/gky955
 46. Anders S, Pyl PT, Huber W. Htseq - a Python Framework to Work With High-Throughput Sequencing Data. *Bioinformatics* (2015) 31:166–9. doi: 10.1093/bioinformatics/btu638
 47. Love MI, Huber W, Anders S. Moderated Estimation of Fold Change and Dispersion for RNA-Seq Data With Deseq2. *Genome Biol* (2014) 15:550. doi: 10.1186/s13059-014-0550-8

48. Durbin BP, Hardin JS, Hawkins DM, Rocke DM. A Variance-Stabilizing Transformation for Gene-Expression Microarray Data. *Bioinformatics* (2002) 18 Suppl 1:S105–10. doi: 10.1093/bioinformatics/18.suppl_1.S105
49. Rue-Albrecht K, McGettigan PA, Hernández B, Nalpas NC, Magee DA, Parnell AC, et al. Goexpress: An R/Bioconductor Package for the Identification and Visualisation of Robust Gene Ontology Signatures Through Supervised Learning of Gene Expression Data. *BMC Bioinf* (2016) 17:126. doi: 10.1186/s12859-016-0971-3
50. Davis S, Meltzer PS. Geoquery: A Bridge Between the Gene Expression Omnibus (GEO) and Bioconductor. *Bioinformatics* (2007) 23:1846–7. doi: 10.1093/bioinformatics/btm254
51. Ammar R, Reinke Breen L. A Murine Systemic Bleomycin Model of Scleroderma. *GSE132869* (2019).
52. Ravanetti F, Ragionieri L, Ciccimarra R, Ruscitti F, Pompilio D, Gazza F, et al. Modeling Pulmonary Fibrosis Through Bleomycin Delivered by Osmotic Minipump: A New Histomorphometric Method of Evaluation. *Am J Physiol Lung Cell Mol Physiol* (2020) 318:L376–85. doi: 10.1152/ajplung.00311.2019
53. Park JK, Coffey NJ, Bodine SP, Zawatsky CN, Jay L, Gahl WA, et al. Bleomycin Induces Drug Efflux in Lungs. A Pitfall for Pharmacological Studies of Pulmonary Fibrosis. *Am J Respir Cell Mol Biol* (2020) 62:178–90. doi: 10.1165/rcmb.2018-0147OC
54. Walters DM, Kleeberger SR. Mouse Models of Bleomycin-Induced Pulmonary Fibrosis. *Curr Protoc Pharmacol* (2008). Chapter 5:Unit 5.46. doi: 10.1002/0471141755.ph0546s40
55. Benjamini Y. Discovering the False Discovery Rate. *J R Stat Soc Ser B Stat Methodol* (2010) 72:405–16. doi: 10.1111/j.1467-9868.2010.00746.x
56. Kendall RT, Feghali-Bostwick CA. Fibroblasts in Fibrosis: Novel Roles and Mediators. *Front Pharmacol* (2014) 5:123. doi: 10.3389/fphar.2014.00123
57. Muro AF, Moretti FA, Moore BB, Yan M, Atrasz RG, Wilke CA, et al. An Essential Role for Fibronectin Extra Type III Domain A in Pulmonary Fibrosis. *Am J Respir Crit Care Med* (2008) 177:638–45. doi: 10.1164/rccm.200708-1291OC
58. Ebener S, Barnowski S, Wotzkow C, Marti TM, Lopez-Rodriguez E, Crestani B, et al. Toll-Like Receptor 4 Activation Attenuates Profibrotic Response in Control Lung Fibroblasts But Not in Fibroblasts From Patients With IPF. *Am J Physiol Lung Cell Mol Physiol* (2017) 312:L42–55. doi: 10.1152/ajplung.00119.2016
59. Liu C, Chen X, Yang L, Kisseleva T, Brenner DA, Seki E. Transcriptional Repression of the Transforming Growth Factor β (Tgf- β) Pseudoreceptor BMP and Activin Membrane-Bound Inhibitor (BAMBI) by Nuclear Factor κ b (Nf- κ b) p50 Enhances TGF- β Signaling in Hepatic Stellate Cells. *J Biol Chem* (2014) 289:7082–91. doi: 10.1074/jbc.M113.543769
60. Bhattacharyya S, Wang W, Qin W, Cheng K, Coulup S, Chavez S, et al. TLR4-Dependent Fibroblast Activation Drives Persistent Organ Fibrosis in Skin and Lung. *JCI Insight* (2018) 3:e98850. doi: 10.1172/jci.insight.98850
61. Cieslik KA, Trial J, Entman ML. Aicar Treatment Reduces Interstitial Fibrosis in Aging Mice: Suppression of the Inflammatory Fibroblast. *J Mol Cell Cardiol* (2017) 111:81–5. doi: 10.1016/j.yjmcc.2017.08.003
62. Boyd DF, Allen EK, Randolph AG, Guo X-ZJ, Weng Y, Sanders CJ, et al. Exuberant Fibroblast Activity Compromises Lung Function Via ADAMTS4. *Nature* (2020) 587:466–71. doi: 10.1038/s41586-020-2877-5
63. Pilling D, Vakil V, Cox N, Gomer RH. Tnf- α -Stimulated Fibroblasts Secrete Lumican to Promote Fibrocyte Differentiation. *Proc Natl Acad Sci* (2015) 112:11929–34. doi: 10.1073/pnas.1507387112
64. Epstein Shochet G, Brook E, Israeli-Shani L, Edelstein E, Shitrit D. Fibroblast Paracrine TNF- α Signaling Elevates Integrin A5 Expression in Idiopathic Pulmonary Fibrosis (IPF). *Respir Res* (2017) 18:122. doi: 10.1186/s12931-017-0606-x
65. Pittet J-F, Koh H, Fang X, Iles K, Christiaans S, Anjun N, et al. HMGB1 Accelerates Alveolar Epithelial Repair Via an IL-1 β - and α v β 6 Integrin-Dependent Activation of TGF- β 1. *PLoS One* (2013) 8:e63907. doi: 10.1371/journal.pone.0063907
66. Sánchez-Tarjuelo R, Cortegano I, Manosalva J, Rodríguez M, Ruíz C, Alía M, et al. The TLR4-MyD88 Signaling Axis Regulates Lung Monocyte Differentiation Pathways in Response to *Streptococcus pneumoniae* Front Immunol (2020) 11:2120. doi: 10.3389/fimmu.2020.02120
67. Hussain S, Johnson CG, Sciruba J, Meng X, Stober VP, Liu C, et al. TLR5 Participates in the TLR4 Receptor Complex and Promotes MyD88-Dependent Signaling in Environmental Lung Injury. *Elife* (2020) 9:e50458. doi: 10.7554/eLife.50458
68. Perros F, Lambrecht BN, Hammad H. TLR4 Signalling in Pulmonary Stromal Cells Is Critical for Inflammation and Immunity in the Airways. *Respir Res* (2011) 12:125. doi: 10.1186/1465-9921-12-125
69. Zhang Y, Wu J, Ying S, Chen G, Wu B, Xu T, et al. Discovery of New MD2 Inhibitor From Chalcone Derivatives With Anti-Inflammatory Effects in LPS-induced Acute Lung Injury. *Sci Rep* (2016) 6:25130. doi: 10.1038/srep25130
70. O'Reilly S, van Laar JM. Targeting the TLR4-MD2 Axis in Systemic Sclerosis. *Nat Rev Rheumatol* (2018) 14:564–6. doi: 10.1038/s41584-018-0077-6
71. Luo S, Gong J, Cao X, Liu S. Ligustilide Modulates Oxidative Stress, Apoptosis, and Immunity to Avoid Pathological Damages in Bleomycin Induced Pulmonary Fibrosis Rats Via Inactivating TLR4/MyD88/NF-KB P65. *Ann Transl Med* (2020) 8:931. doi: 10.21037/atm-20-4233
72. Xu G-R, Zhang C, Yang H-X, Sun J-H, Zhang Y, Yao T-T, et al. Modified Citrus Pectin Ameliorates Myocardial Fibrosis and Inflammation Via Suppressing Galectin-3 and TLR4/Myd88/NF-kb Signaling Pathway. *BioMed Pharmacother* (2020) 126:110071. doi: 10.1016/j.biopha.2020.110071
73. Ma J-Q, Zhang Y-J, Tian Z-K, Liu C-M. Bixin Attenuates Carbon Tetrachloride Induced Oxidative Stress, Inflammation and Fibrosis in Kidney by Regulating the Nrf2/TLR4/MyD88 and PPAR- γ /Tgf- β 1/Smad3 Pathway. *Int Immunopharmacol* (2021) 90:107117. doi: 10.1016/j.intimp.2020.107117
74. Varga J, Trojanowska M, Kuwana M. Pathogenesis of Systemic Sclerosis: Recent Insights of Molecular and Cellular Mechanisms and Therapeutic Opportunities. *J Scleroderma Relat Disord* (2017) 2:137–52. doi: 10.5301/jsrd.5000249
75. Tatler AL, Jenkins G. Tgf- β Activation and Lung Fibrosis. *Proc Am Thorac Soc* (2012) 9:130–6. doi: 10.1513/pats.201201-003AW
76. Fernandez IE, Eickelberg O. The Impact of TGF- β on Lung Fibrosis: From Targeting to Biomarkers. *Proc Am Thorac Soc* (2012) 9:111–6. doi: 10.1513/pats.201203-023AW
77. Chanda D, Otoupalova E, Smith SR, Volckaert T, De Langhe SP, Thannickal VJ. Developmental Pathways in the Pathogenesis of Lung Fibrosis. *Mol Aspects Med* (2019) 65:56–69. doi: 10.1016/j.mam.2018.08.004
78. Bhattacharyya S, Tamaki Z, Wang W, Hinchcliff M, Hoover P, Getsios S, et al. Fibronectin/EDA Promotes Chronic Cutaneous Fibrosis Through Toll-like Receptor Signaling. *Sci Transl Med* (2014) 6:232ra50. doi: 10.1126/scitranslmed.3008264
79. Bhattacharyya S, Wang W, Morales-Nebreda L, Feng G, Wu M, Zhou X, et al. Tenascin-C Drives Persistence of Organ Fibrosis. *Nat Commun* (2016) 7:11703. doi: 10.1038/ncomms11703
80. Izbicki G, Segel MJ, Christensen TG, Conner MW, Breuer R. Time Course of Bleomycin-Induced Lung Fibrosis. *Int J Exp Pathol* (2002) 83:111–9. doi: 10.1046/j.1365-2613.2002.00220.x
81. Cho JW, Jung H, Lee MJ, Lee SH, Lee SH, Mun YH, et al. Preparedness of Personal Protective Equipment and Implementation of New CPR Strategies for Patients With Out-of-Hospital Cardiac Arrest in the COVID-19 Era. *Resusc Plus* (2020) 3:100015. doi: 10.1016/j.resplu.2020.100015
82. McGinn JT, Aziz M, Zhang F, Yang W-L, Nicastro JM, Coppa GF, et al. Cold-Inducible RNA-binding Protein-Derived Peptide C23 Attenuates Inflammation and Tissue Injury in a Murine Model of Intestinal Ischemia-Reperfusion. *Surgery* (2018) 164:1191–7. doi: 10.1016/j.surg.2018.06.048
83. Ode Y, Aziz M, Wang P. CIRP Increases ICAM-1 Phenotype of Neutrophils Exhibiting Elevated iNOS and NETs in Sepsis. *J Leukocyte Biol* (2018) 103:693–707. doi: 10.1002/jlb.3a0817-327rr
84. Zhou M, Yang W-L, Ji Y, Qiang X, Wang P. Cold-Inducible RNA-binding Protein Mediates Neuroinflammation in Cerebral Ischemia. *Biochim Biophys Acta* (2014) 1840:2253–61. doi: 10.1016/j.bbagen.2014.02.027
85. Torii K, Kubota A, Araki T, Endo M. Time-Series Single-Cell RNA-Seq Data Reveal Auxin Fluctuation During Endocycle. *Plant Cell Physiol* (2020) 61:243–54. doi: 10.1093/pcp/pcz228
86. McIntyre LM, Lopiano KK, Morse AM, Amin V, Oberg AL, Young LJ, et al. RNA-Seq: Technical Variability and Sampling. *BMC Genomics* (2011) 12:293. doi: 10.1186/1471-2164-12-293
87. Liu Y, Zhou J, White KP. RNA-Seq Differential Expression Studies: More Sequence or More Replication? *Bioinformatics* (2014) 30:301–4. doi: 10.1093/bioinformatics/btt688
88. Lee R, Reese C, Bonner M, Tourkina E, Hajdu Z, Riemer EC, et al. Bleomycin Delivery by Osmotic Minipump: Similarity to Human Scleroderma Interstitial Lung Disease. *Am J Physiol Lung Cell Mol Physiol* (2014) 306:L736–48. doi: 10.1152/ajplung.00210.2013
89. Singh B, Kasam RK, Sontake V, Wynn TA, Madala SK. Repetitive Intradermal Bleomycin Injections Evoke T-helper Cell 2 Cytokine-Driven Pulmonary

Fibrosis. *Am J Physiol Lung Cell Mol Physiol* (2017) 313:L796–806. (2012) doi: 10.1164/ajrccm-conference.2012.185.1_meetingabstracts.a5535

Conflict of Interest: The authors declare that the research was conducted in the absence of any commercial or financial relationships that could be construed as a potential conflict of interest.

Publisher's Note: All claims expressed in this article are solely those of the authors and do not necessarily represent those of their affiliated organizations, or those of the publisher, the editors and the reviewers. Any product that may be evaluated in

this article, or claim that may be made by its manufacturer, is not guaranteed or endorsed by the publisher.

Copyright © 2021 Bolourani, Sari, Brenner and Wang. This is an open-access article distributed under the terms of the Creative Commons Attribution License (CC BY). The use, distribution or reproduction in other forums is permitted, provided the original author(s) and the copyright owner(s) are credited and that the original publication in this journal is cited, in accordance with accepted academic practice. No use, distribution or reproduction is permitted which does not comply with these terms.